PMAS

Vol. 63 No 04(248) 2023

DOI: https://doi.org/10.5564/pmas.v63i04.3430

ARTICLE

Pc1 hydromagnetic emissions of chevron type

Parkhomov Vladimir Alexandrovich[1]*, Tsegmed Battuulai[2], Dovbnya Boris Victorovich[3], Khomutov Sergey Yurievich[4], Eselevich Victor Grigorieivich[5] and Glinskyi Igor Yurievich[6]

[1] Department of Mathematical Methods and Digital Technologies, Baikal State University, Irkutsk, Russia
[2] Department of Geomagnetism, Institute of Geophysics and Astronomy, Mongolian Academy of Sciences, Ulaanbaatar, Mongolia
[3]Borok Geophysical Observatory, O.Yu. Schmidt Institute of Physics of the Earth, Russian Academy of Sciences, Russia
[4] Geophysical Observatory Paratunka, Institute of Cosmophysical Research and Radio Wave Propagation, of the Far Eastern Branch, Russian Academy of Sciences, (IKIR) FEB RAS),Russia
[5]Department of Solar Physics, Institute of Solar-Terrestrial Physics, Siberian Branch (ISTP SB), Russian Academy of Sciences, Irkutsk, Russia
[6] Faculty of Mathematical Methods and Computational Techniques, Baikal State University, Irkutsk, Russia

ARTICLE INFO: Received: 11 Nov, 2023; Accepted: 29 Nov, 2023

Abstract: The article presents the results of studying novel bursts of ULF emissions within 0.5–2.5 Hz (Pc1 geomagnetic pulsations) with a simultaneous increase (~0.01 Hz/min) and decrease in frequency (~0.01 Hz/min) lagging by ~5÷10 min from the initial mean frequency (~0.6 Hz). From their formal resemblance with the stripes on military officer uniforms, these emissions are called Pc1 chevrons. The bursts were observed during strong short-term geomagnetic disturbances (~1 hour): substorms with high gradient of ionospheric currents+ intensification (dD/dt or dH/dt ~1–1.3 nT/s).

We present the main parameters and couplings of these emissions with substorm geophysical phenomena of 11.02.1985, 06.04.1997 and 18.07.2013 events. Polar satellite observations of auroras are compared with LANL-91, 94 and THEMIS-A observations of charged particle fluxes. Possible mechanisms generating oscillations are also discussed.

Keywords:*Pc1geomagnetic pulsations, frequency separation of spectrum, substorm, ion fluxes, particle drift from the magnetotail, wave- particle interaction;*

INTRODUCTION

According to international classification, geomagnetic pulsations (Ultra-Low Frequence (ULF) emissions) in the period range of 0.2–5 s (0.2–5 Hz) are designated as Pc1 [1].

***Corresponding author, email**: pekines_41@mail.ru* *https://orcid.org/0000-0004-0637-8979*

Vol. 63 No 04(248) 2023
DOI: https://doi.org/10.5564/pmas.v63i04.3430

A huge number of articles and monographs deal with emissions of this type, since Sucksdorf [23] discovered them in 1932. Basic results of investigations into pulsations of this type are summarized in monographs and reviews [1-4].

In Pc1 frequency range, different types of emissions are observed; they have different spectra, types and patterns of amplitude modulation, generation time and couplings with other geophysical phenomena. One of the first Pc1 classifications, called hydromagnetic emissions, by the type of dynamic spectra (sonogram), can be found in [4]. Here, based on 3,035 observations of hydromagnetic emissions at Syowa Observatory in Antarctica (L~6), 12 types of spectral structures are identified and diagrams of their daily distribution are plotted.

From observations of geomagnetic pulsations at Vostok Observatory in the south polar cap and at SP-22 drifting station in the north polar cap, 13 types of dynamic spectra (sonogram) of MHD emissions in Pc1 frequency range were identified and described briefly in monograph [2].

Among plentiful types of emissions, there are ones with rising (IPDP – irregular pulsations of diminishing period), falling or not changing frequency (Pc1-2 band) [4], but no events were reported, in which data of ground-based recording would show emissions with a simultaneous rise and fall in emission frequency in one event. At the same time, some papers report registration of these emissions on satellites [5], stating that in the events observed, these emissions demonstrate frequency chirping. Note the main feature of the cited results – the described signals have a short duration of ~1 min, which is probably due to satellite motion. In [14, 15], events in higher frequency range (ELF 10–1500 Hz) of emissions after midnight (chorus) at L=5÷9 were investigated. In [16], the author considered the rising and falling tones related to electronic cyclotron harmonic waves observed with the Van Allen probes. In Russian literature, the term "chevron" is used for this physical concept (frequency chirping). For the sake of brevity and convenience, in further description of these emissions, we will call them "chevron" emissions, with reference to similarity of the observed phenomenon and the term description in Wikipedia. Chevron is a V—shaped graphic symbol comprising two segments with the ends joining at an angle, similar to Latin letter V, rotated in a variety of ways. We will consider events, in which V lies in the horizontal plane. Note the conditionality of this definition, since in Pc1 chevrons, the frequency descending branch is shorter in duration than the ascending one.

MATERIALS AND METHODS

Data and methods of processing

In this study, we used data from induction magnetometers installed in observatories Borok (58.0° N, 39.0° E), Mondy (51.6° N, 100.8° E), Magadan (53.34° N, 150.46° E), Paratunka (53.02° N, 158.65° E), standard magnetograms from observatories Irkutsk (52.18°N, 104.18° E), Tixie (71.36° N, 128.52° E), Dixon (73.61° N, 80.19° E). Before 2001, induction magnetometers with 10 Hz quantization frequency and time correction via GPS system were operated at Borok and Mondy observatories. Beginning from 2010, geomagnetic filed variations are

Vol. 63 No 04(248) 2023
DOI: https://doi.org/10.5564/pmas.v63i04.3430

registered with 64 Hz quantization frequency at Mondy observatory, and since 2013 - at Magadan and Paratunka observatories.

Spectral analysis was carried out using programs Spectra PLUS [7], spectral–temporal analysis (STAN) [8] and spectrograms original signal digital data obtained with an induction magnetometer. Spectra PLUS enables FFT analysis (also known as fast Fourier transform) of audio signals. Accordingly, the program first converts digital data in audio format into wave-files with high resolution, after which it calculates signal spectrograms.

Methods for calculting signal spectral characteristics differ as follows:

1. Spectrograms use a time window of a certain duration, which moves along the entire length of data and calculates spectra for each selected window.
2. In STAN, signal spectrum is first calculated for the entire array of data processed. From data profile, a frequency window of a certain frequency range is applied, and inverse Fourier transform is performed in the section selected.

Thus, spectral images in spectrograms are plotted from the identified signal spectral power, and in STAN — from signal intensity at certain frequencies.

To estimate signal polarization, initial data are presented in the form of complex numbers, where one component represents a real part, and another component represents an imaginary part of horizontal transverse electromagnetic oscillations [13].

$$s(t) = x(t) + jy(t)$$

For any angular frequency ω one gets two complex Fourier coefficients, one for the negative frequency $\omega -$ and the other for positive frequency $\omega +$. It is convenient to present the coefficients in polar coordinates. Parameters of the original signal polarization are set by Fourier transforms $S(\omega+)$ and $S(\omega-)$.

$$S(\omega -) = r_- \exp(i\theta); \qquad S(\omega +) = r_+ \exp(i\theta);$$

The ellipticity, sense of rotation, and orientation of major axis of the polarization ellipse are easily represented as a function of frequency.

Ellipticity ε equals: $\varepsilon = (r_+ - r_-)/(r_+ + r_-)$.

Sense of rotation: $K = sign(r_+ + r_-)$, where negative value means right-handed rotation.

The major half axis: $A = (r_+ - r_-)$.

Total power: $P = 2r_+^2 + 2r_-^2$.

To estimate signal polarization, initial data are presented in the form of complex numbers, where one component represents a real part, and another component represents an imaginary part of horizontal transverse electromagnetic oscillations [13]. Then we divide the original signal into two other complex signals $s+$ and $s-$ of opposite polarities and study the correspondence existing between $s+$ and $s-$ and the analytical signal concept. Parameters of the original signal polarization are set by very simple expressions through $s+$ or $s-$ or their Fourier transforms $s+$ and $s-$. When Fourier analysis is performed for $s+$ and $s-$, the ellipticity, sense of rotation, and orientation of major axis of the polarization ellipse are easily represented as a function of frequency.

Vol. 63 No 04(248) 2023
DOI: https://doi.org/10.5564/pmas.v63i04.3430

RESULTS

Morphology of 06.04.1997 Pc1 chevron

An unusual emission with a simultaneous frequency rise (~0.01 Hz/min) and fall (~0.01 Hz/min) from the initial mean frequency of ~0.58 Hz, was clearly seen at Borok Observatory (Figures 1a,b) on the day after a pronounced burst of irregular pulsations PiB (Pi1-2), which is a generally recognized indicator of substorm explosive phase. At Mondy Observatory located ~70° eastward, only a descending frequency branch was seen (Figure 1d). At Borok Observatory (Figures 1a,b), the emission begins at ~16.23 UT at the mean frequency of ~0.58 Hz. The mean frequency in time interval Δt ~4 min remains unchanged, and then, there occurs a simultaneous rise (up to ~1.1 Hz) during ~23 min and a fall in frequency (down to ~0.6 Hz) during ~11 min**.** Most distinctively, the shape of emission in the form of two branches – with falling and rising frequency is visible at Borok Observatory (Figures 1a, b). Moreover, the ascending branch is longer in duration than the descending branch. At Mondy Observatory, one can see faint traces of the emission descending branch.

Figure 1 polarogram shows polarization properties of oscillations. One can see most clearly that polarized oscillations are distinguished at Borok Observatory (Figures 1c, d), while at Mondy Observatory, there are no polarized oscillations. The ascending branch of the pulsation burst is of right-handed polarization (Figure 1c), and for the descending branch, polarization is not distinctive. At Mondy Observatory, there are no polarized oscillations, although Figure 2d shows an increase in the signal spectral power of the descending branch along the geomagnetic field horizontal components, which we represent as $H = X + iY$. Thus, using the above polarogram, it is difficult to positively subsume the observed polarization oscillations under any type of polarized waves.

Figures 2a, b, c, d, e show geophysical phenomena comprising the substorm. Figure 1 shows emission with a duration of ~26 min that was observed against the background of moderate geomagnetic activity (Kp15–18 = 3+) in the recovery phase of a strong short-term (~50 min) substorm (AEmax = 830 nT) with four activations in the form of Pi2 geomagnetic pulsation bursts detected at observatories Yakutsk and Borok within the longitudes ~91° (not shown).

First of all, STANogram of geomagnetic pulsations in the period range 0.6–200 s shows a classic picture of the regime of irregular geomagnetic pulsations at mid-latitudes in near-midnight hours local time. The chevron appearance is preceded by the generation of a broadband burst of PiB (Pi1-2) pulsations (arrow in Figure 2). Most clearly, this chevron is visible at Borok Observatory.

Let's consider the substorm features in auroras in the UV range on satellite Polar [9]. Faint glow at 16:03 UT in the midnight sector within latitudes 60°–70° enhances suddenly at 16:13 UT, and at 16:19, auroral breakup is visible in latitudinal range of ~20°. At 16:28 UT, the western auroral bend reaches the evening meridian (~19 MLT), and at 16:34 UT, the remaining one only brighten in the evening sector, and the auroral zone diffuse glows between the evening and morning meridians.

Vol. 63 No 04(248) 2023
DOI: https://doi.org/10.5564/pmas.v63i04.3430

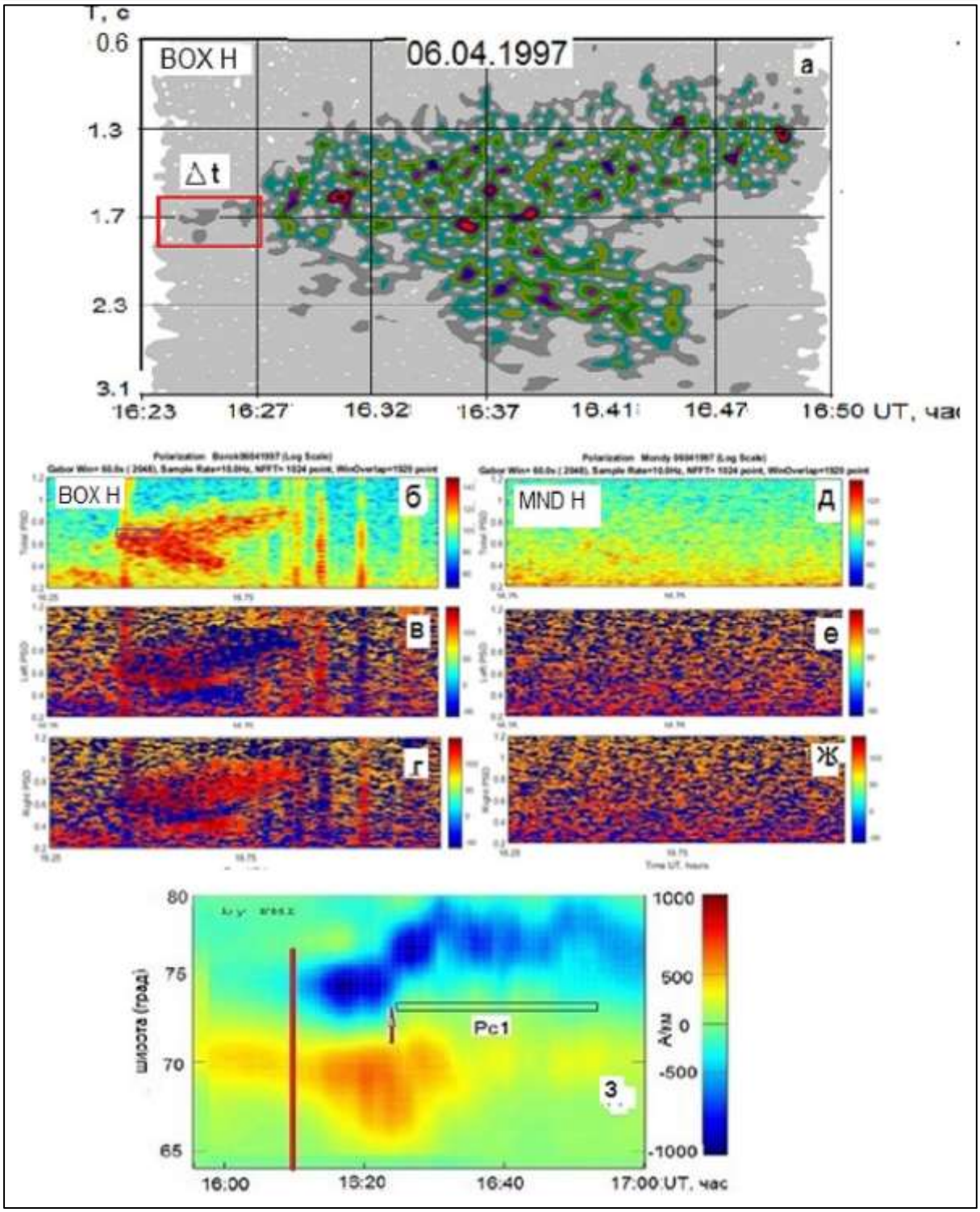

Figure 1. (a) Pc1 chevron STANogram at Borok Observatory (MLT = UT+3); (b) Polarogram of geomagnetic pulsations in the same place; (c) Left-handed polarization (L-wave); (d) Right-handed polarization (R-wave); (e, f, g) Same at obs. Mondy (MLT = UT+7). Δt is the initial phase with the mean frequency unchanged; (h) Current system model calculation from data by IMAGE magnetometer meridional network during generation of Pc1 chevron. Orange color – eastern electrojet, blue color – western electrojet

Vol. 63 No 04(248) 2023
DOI: https://doi.org/10.5564/pmas.v63i04.3430

The beginning of Pc1 chevron at ~16.26 UT is recorded in the substorm decay phase in auroras.

Variations in local *IL*-index of auroral activity from IMAGE magnetometer network (Figure 2d) rise dramatically from ~10 nT to ~500 nT within ~10 min, and then they decay in a wavelike manner. Dynamics of the index variations is determined by variations in western current (Figures 1h, 2d, e), which fluctuates and moves northward. The onset of Pc1 chevron generation coincides with the moment of eastern current weakening and northward throw of the western current (vertical arrow in Figure 1h), which is attributed to approach of the plasma sheet inner edge to the Earth[19].

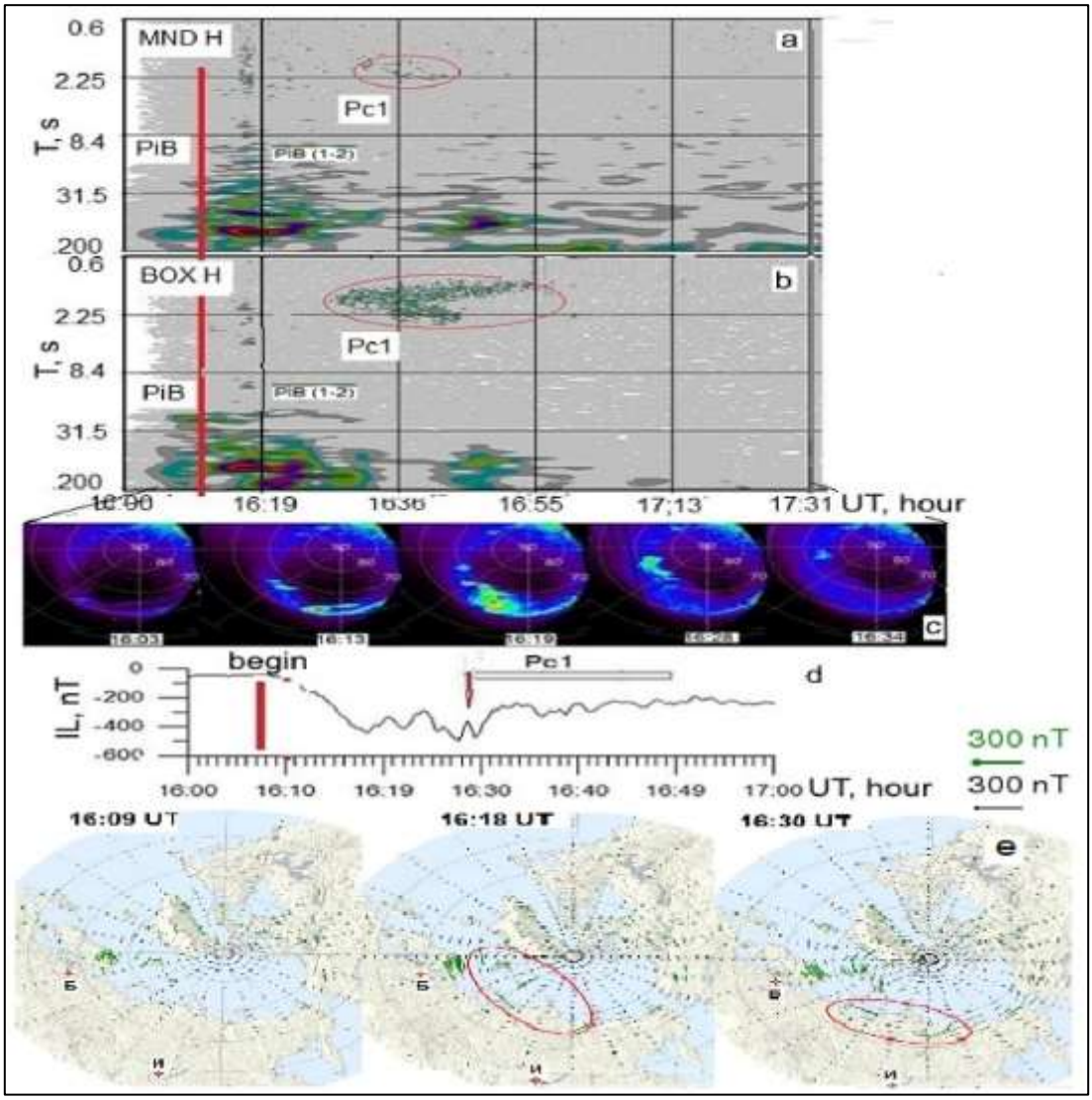

Figure 2. Geophysical phenomena accompanying generation of Pc1 chevron. (a) STANogram, Mondy Observatory, chevron is marked with Pc1 red oval; (b) STANogram, Borok Observatory, Pc1 red oval marks the chevron. Initial phase Δt is marked with red rectangle in Figure 1a; (c) Sequence of Polar satellite images of auroras; (d) IL index variation from IMAGE network; (e) Equivalent current systems demonstrating enhancement of the western current in longitudinal range 20°–100° (Bear Island BJN – Tixie TIX)

Vol. 63 No 04(248) 2023
DOI: https://doi.org/10.5564/pmas.v63i04.3430

Thus, the dynamics of phenomena observed is close to the phenomena comprising the substorm explosive phase (breakup) [12]. From ground data, the main feature of the considered substorm, during which Pc1 chevron is generated, is its explosive development within ~10 min, the rate of geomagnetic field *H*-component variation reaches ~1 nT/s, the onset of ULF signal generation coincides with the moment of northward throw of western electrojet, rapid spatial expansion of glow region, a sudden enhancement of western electrojet in the evening sector (~19 MLT) (*IL* index increases by ~500 nT). The main distinction of geomagnetic pulsation mode is that a substorm explosive phase is usually accompanied by a broadband burst of PiB (Pi1B + Pi2), which is normally followed by bursts with rising frequency (IPDP).

But in the case addressed, we can see the spectrum separation and appearance of a falling frequency branch. According to Horita et al. [22], only 40–60 keV protons are effective for generating ion cyclotron waves in IPDP frequency range, so let us consider satellite observations of particle fluxes in this time interval.

Satellite observations of charged particle fluxes

Geostationary satellite LANL-91 longitudinally was between Borok and Mondy observatories (Re=6.614, φ=1.718°, λ=69.22°), and LANL-94 was located eastward from Mondy (Re=6.615, φ=-0.741°, λ=103.1°), in the central part of the midnight plasma sheet.

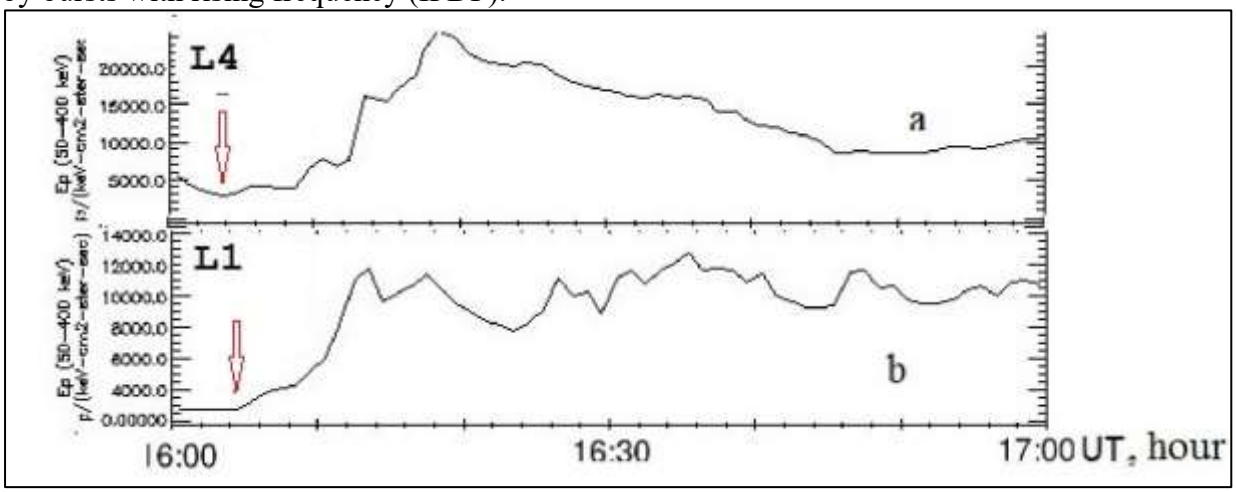

Figure 3. Variations in proton flux densities (a, b) on LANL-91 and LANL-94 geostationary satellites. Red arrows indicate arrival of the substorm disturbed particle flux

As can be seen in Figure 3 (panels a, b), at 16.09 UT, 50–400 KeV proton fluxes increase drastically on LANL-94 (L-4) and LANL-91(L-1) [https://cdaweb.gsfc.nasa.gov/cdaweb/istp_public/] located in the plasma sheet night region of the magnetotail at the distance of ~6Re. These fluxes can be related to the particles accelerated during the substorm and moving towards the Earth.

It should be noted that despite close location, Interball-Auroral satellite did not observe enhancement of the particle flux; and on Polar, there was no noticeable increase in proton density, but at 16.12 UT, electron density increased from 0.02 to 0.07 cm^{-3}.

At 16.17 UT, on their dayside, geostationary satellites GOES-8 and GOES-9

Vol. 63 No 04(248) 2023
DOI: https://doi.org/10.5564/pmas.v63i04.3430

[https://cdaweb.gsfc.nasa.gov/cdaweb/istp_public/registered] registered drastic increases in diffuse fluxes of high-energy protons with *E*p = 0.7–4 MeV (Fig. 4a,c) and the onset of the geomagnetic field *H*n normal component falling simultaneously on two satellites (Figures 4b,d), which can be attributed to the manifestation of substorm ionospheric currents on the dayside. Note that the onset of proton flux growth on LANL-91 and LANL-94 nightside gets ahead of the onset of disturbance on the dayside of satellites, which is recorded at 16:04 UT (Figure 4 red arrow). This ~13 min lag in proton flux growth is probably due to plasma motion from the nightside to dayside. The described phenomenon can be explained within a substorm model [17, 18]. According to this model, "a part of the substance and energy that did not dissipate into the ionosphere during precipitation and supply of ionospheric currents, is brought to the magnetosphere forepart into the anticonvective jet."

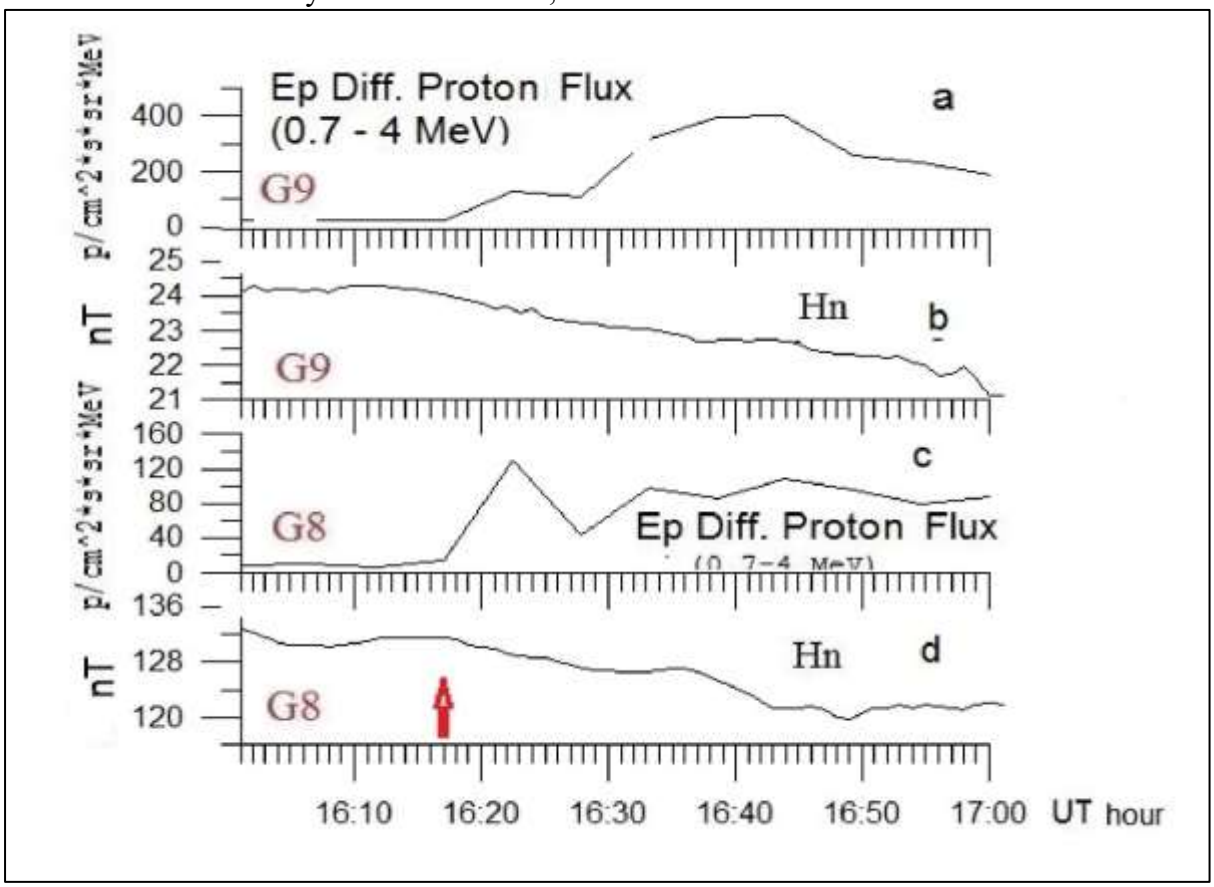

Figure 4. Variations in geomagnetic field (a, b) and proton fluxes (c, d) on geostationary satellites GOES 8, 9. Arrow indicates onset of proton flux enhancement and geomagnetic field disturbance

Summarizing the phenomena of the geophysical situation, during which the Pc1 chevron is detected, we can conclude that emission of this type is clearly associated with a substorm and correlates with pulse processes in the decay phase with fast motion of particles from the magnetotail. Pc1 chevron is a combination of emissions of two types: one with a constant mean frequency similar to IPDP onset [3, 4], and another one with a falling frequency resembles the emissions detected in [11] and associated with the penetration of alpha

Vol. 63 No 04(248) 2023
DOI: https://doi.org/10.5564/pmas.v63i04.3430

particles into the magnetosphere during pulse processes in the magnetosheath.

The 18.07.2013 event

Pc1 chevron was confidently observed only at Mondy Observatory (Figures 5 a, b). Note the main feature of a chevron structure. In Figures 1, 2, 5, a chevron comprises two components – initially, the mean frequency is unchanged, and over time Δt ~10 min, branches appear with frequency rise and fall, in which one can see structural elements similar to those of Pc1, but with not so clearly expressed positive frequency dispersion. Significantly, the branch of falling frequency oscillations is of shorter duration than the rising frequency branch in all events considered.

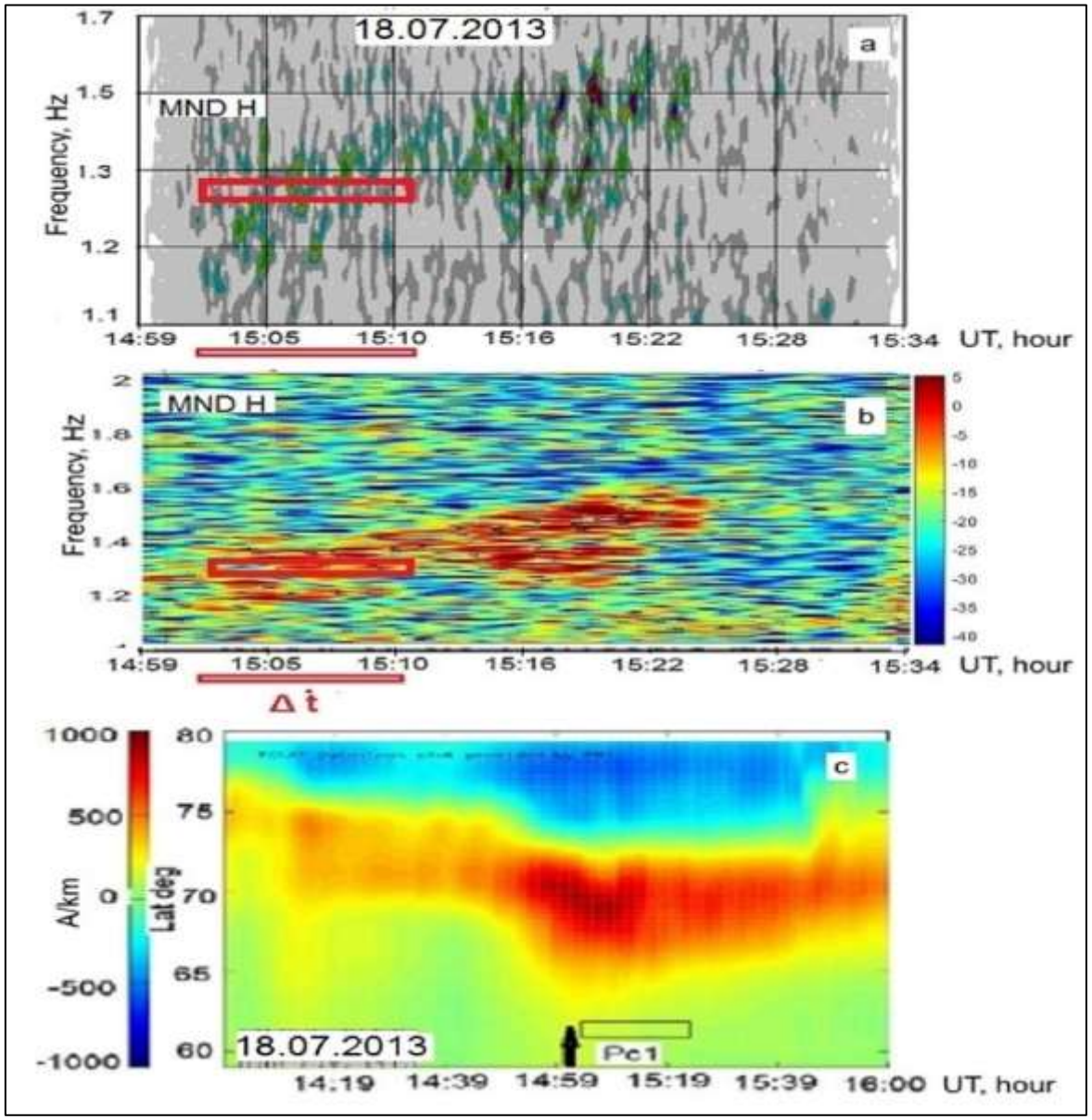

Figure 5. (a) STANogram; (b) Spectrogram of Pc1 chevron on 18.07.2013; (c) Current system model calculation from data by IMAGE magnetometer network during generation of Pc1 chevron. Orange color – eastern electrojet and blue color – western electrojet. Δt — duration of the chevron first phase with the mean frequency unchanged

Vol. 63 No 04(248) 2023
DOI: https://doi.org/10.5564/pmas.v63i04.3430

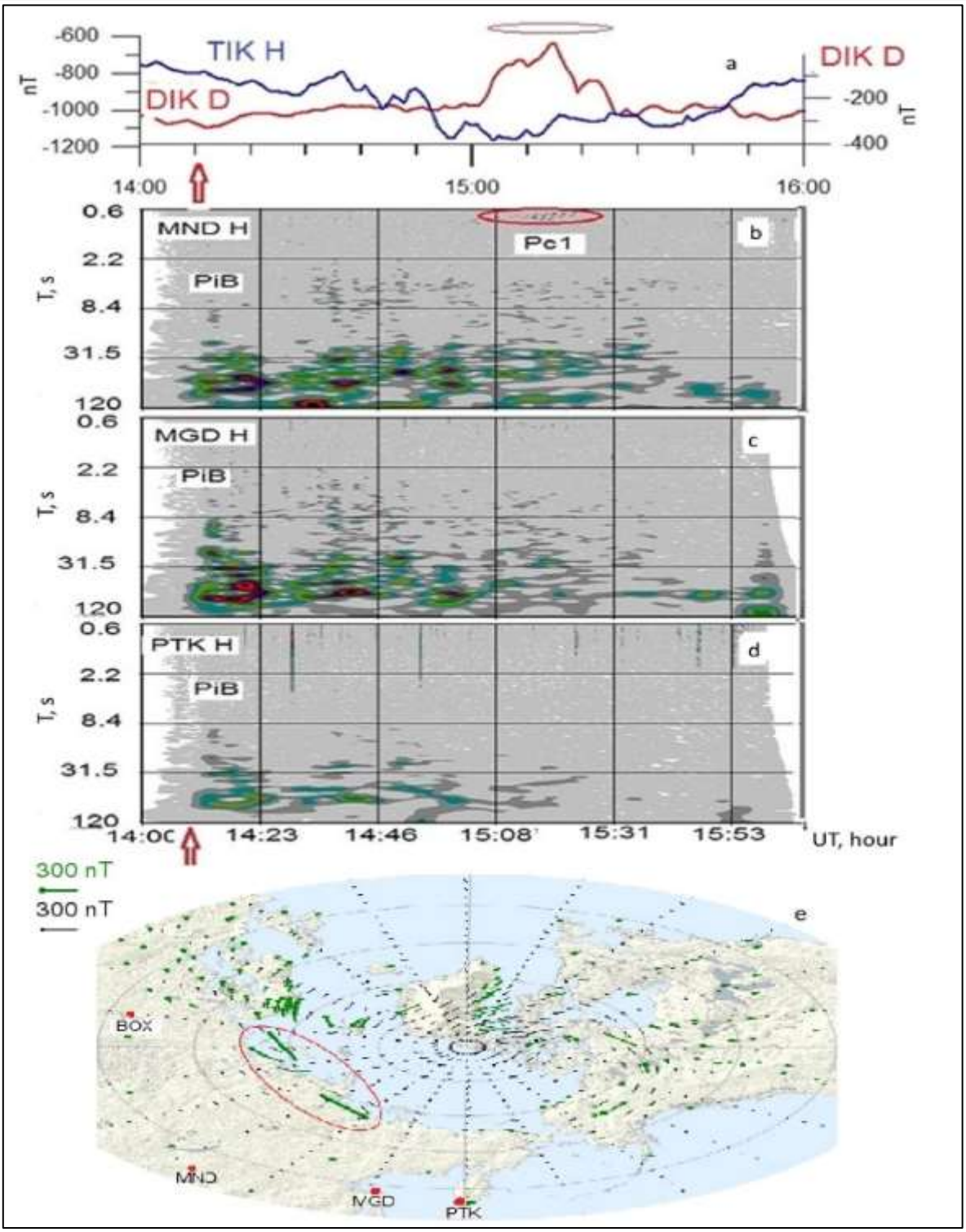

Figure 6. Geophysical situation during registration of Pc1 chevron on 18.07.2013. a — Fragments of magnetograms from Tixie and Dixon observatories. Arrow — substorm onset. Ellipse — interval of Pc1 chevron observation. b — spectrogram of geomagnetic pulsations at Mondy Observatory. Ellipse — interval of Pc1 chevron observation. c, d — spectrograms of geomagnetic pulsations at observatories Magadan and Paratunka. One can see bursts of PiB irregular geomagnetic pulsations that usually accompany substorms. e — system of equivalent currents

Vol. 63 No 04(248) 2023
DOI: https://doi.org/10.5564/pmas.v63i04.3430

Figure 6 shows geophysical conditions on 18.07.2013 when the chevron was observed, and they are similar to conditions during other events addressed. The chevron was observed on the day with a high magnetic activity (Kp = +5) against the background of the substorm, which, according to [10], had several activations (13:38, 14:33, 14:54 UT). Given here are the following: a - fragments of standard magnetograms at two auroral observatories Tixie and Dixon; b, c, d — spectrograms of three observatories. Spectrograms at ~14:15 UT show broadband bursts of PiB (Pi2+Pi1) pulsations, which are generally recognized indicators of the onset of the substorm explosive phase in longitudinal sector of Mondy – Paratunka (~100°–158°) at 14:54 UT. This moment coincides with the beginning of negative magnetic bay at Tixie Observatory (marked with the arrow in Figure 6a).

At Dixon observatory, whose longitude is close to that of the observatory where Pc1 chevron was registered, at 15:02 UT we can see a large and dramatic jump of meridional D-component of the auroral electrojet by ~400 nT. The beginning of chevron coincides with that of auroral current dramatic change and expansion on IMAGE evening meridian (Figure 5), which coincides with the regularities of chevron generation for other cases considered.

Observations of ion fluxes [20] at 1–10 keV energies in the magnetotail almost on the plasma sheet axis at the distance of ~10.6Re revealed sudden density fluctuations (Figure 7a), energy flux (Figure 7b), temperature anisotropy of protons moving earthward (Figure 7c) and fluctuation of geomagnetic field with frequency near average of chevron frequency.

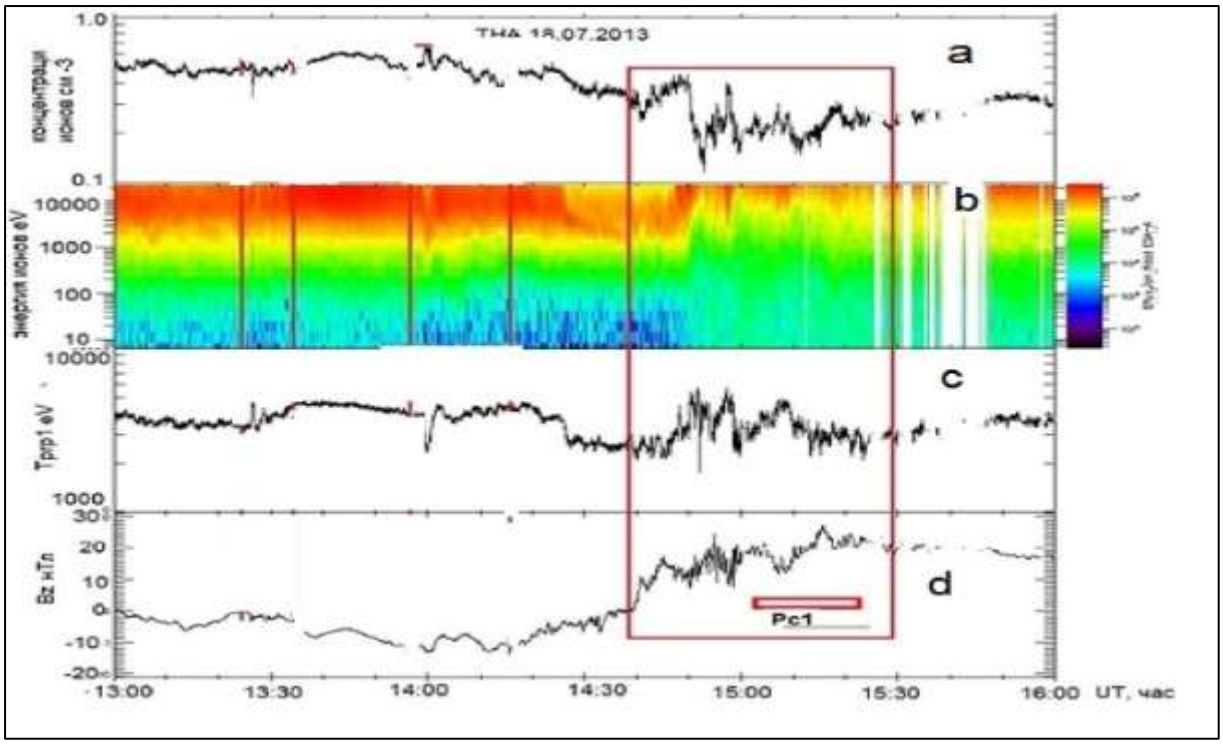

Figure 7. THEMIS-A observations of ion fluxes generated during substorm in the magnetotail. Interval of Pc1 chevron observation is marked with a rectangle. a — ion density variations; b — energy flux spectrogram; c —diagonalized ion temperature (Tprp1 — temperature along magnetic field); d – Bz component of geomagnetic field. Red bold rectangle duration of Pc1 chevron

Vol. 63 No 04(248) 2023
DOI: https://doi.org/10.5564/pmas.v63i04.3430

The 11.02.1985 event

Another Pc1 chevron was registered on February 11, 1985 (Figures 8, a-d). On Figure 8a is the current system model calculation from data by IMAGE magnetometer network during generation of Pc1 chevron. Spectrogram of Pc1 chevron on 11.02.1985 done on Figure 8b (*dt* — duration of the chevron first phase with the mean frequency unchanged). Emission begins at a frequency of ~0.76 Hz. The geophysical situation during the observation of the chevron is similar to the situation during the observation of the chevron on 04.06.1997 As in the first case, the frequency decreasing branch is shorter than the duration of the frequency increasing branch (Figure 8b). In that day in the interval under consideration, a short-term substorm occurs with a sharp increase of AE index (180 nT/min) and in the eastern direction current at the moment of spectrum splitting (Figures 8 a, c, d). To our regret, in this case data about western electrojet is absent because they are not observed on Svalbard net magnetometers.

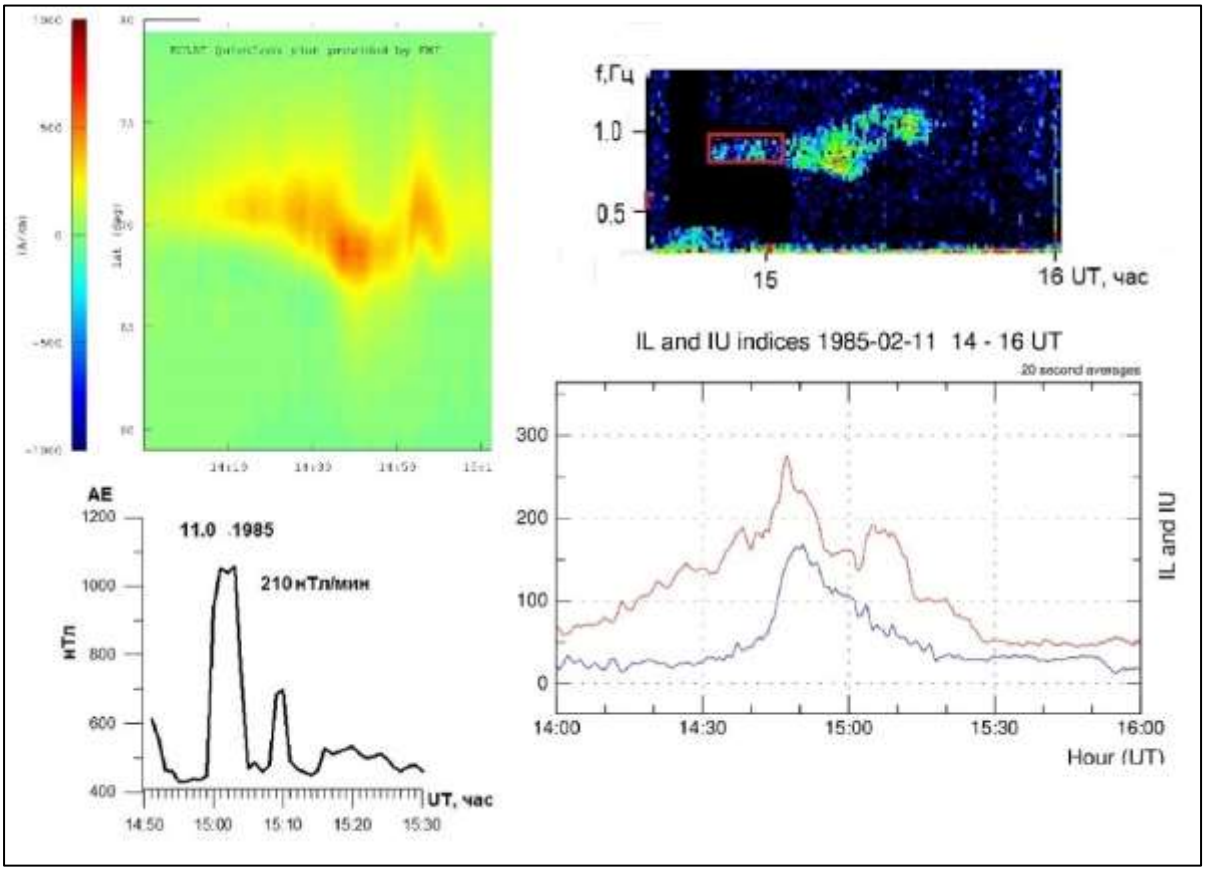

Figure 8. Geophysical situation condition during registration observation of Pc1 chevron on 11.02.1985. (a)Current system model calculation from data by IMAGE magnetometer network during generation of Pc1 chevron. Orange color – eastern electrojet. In this case western electrojet is absent because it is not observed on Svalbard net magnetometers (b) Spectrogram of Pc1 chevron on 11.02.1985; (c) The variation of AE index during of event; (d) Local index IL and UL from data by IMAGE magnetometer network; dt — duration of the chevron first phase with the mean frequencyunchanged.
[https://space.fmi.fi/image/www/index.php?page=il_index]

Vol. 63 No 04(248) 2023
DOI: https://doi.org/10.5564/pmas.v63i04.3430

DISCUSSION AND CONCLUTIONS

1. During moderate (Kp>3) and high magnetic activity (Kp>5), a novel type of ULF emission was detected within 0.5–2.5 Hz of Pc1 geomagnetic pulsations. Two stages of emissions are registered. In the initial stage (0–10 min), the mean frequency remains unchanged, and after Δt ~10 min, the spectrum is separated and there appear regions with the frequency rise and fall, where we can see Pc1 structural elements with positive frequency dispersion. In duration, the falling frequency branch is shorter than the rising frequency branch. Designation "Pc1 chevrons" is proposed for these emissions similar to insignia on military uniforms.
2. Emissions such as “EMIC wave chirping" have repeatedly been registered on satellites [5], where a model of these emissions is presented. The model explains both EMIC wave branches by interaction with magnetospheric plasma at different stages of wave packet propagation along the geomagnetic field line and compares emission parameters only from satellite observations. Therefore, the task is to compare the results of the ground-based and satellite-based observations.
3. In chevrons that are predominantly registered during strong substorms, one can see a rising frequency branch, similar to emissions of IPDP type, and structural elements similar to Pc1. Therefore, it can be assumed that the appearance of Pc1 chevrons with injections of high-energy plasma from the magnetotail (Figure 7) is related to its azimuthal drift to the dayside.
4. We compared timing of dynamic spectra of oscillations on the Earth and LANL-1994 and THEMIS-A onboard records of changes in the intensity and anisotropy of charged particles, in accordance with [21] we assumed that the burst of ion-cyclotron waves resulted from ion-cyclotron instability of the ion flux moving Earthward from the ion tail, which matches the picture of the substorm development [18]. The chevron was registered on the Earth ~15 min after the ion flux drastic change on THEMIS-A (Figure 7). At the same time, the shape of the burst dynamic spectrum is not typical for ion-cyclotron waves due to the existence of spectrum frequency separation. This problem needs to be studied further.

Acknowledgments

The authors express their profound gratitude to A.V. Guglielmi and A.S. Potapov for helpful discussions, B.I. Klain for assistance in processing materials, to D.G. Baishev for discussion and submission of Yakutsk Observatory data. We also thank M.V. Eselevich for his interest in the study.

The authors express their sincere gratitude to NASA CDAWEB for providing satellite data from Wind, Polar, GOES-8, GOES-9, LANL-94, 91, and THEMIS. We thank the managers, developers of instruments and chief designers of experiments conducted on these satellites for the opportunity to use their data. The results are obtained using the equipment of

Vol. 63 No 04(248) 2023
DOI: https://doi.org/10.5564/pmas.v63i04.3430

Shared Equipment Center Angara [http://ckp-rf.ru/ckp/3056]. The work of V.A. Parkhomov is carried out within the state budget research topic of Baikal State University for 2022–2024 "System analysis and methods for information processing". The work of S.Yu. Khomutov is carried out within the implementation of the state assignment no. AAAA-A21-121011290003-0. Measurements with induction magnetometers at Magadan and Paratunka observatories are carried out under the Agreement on Academic Exchange between IKIR FEB RAS and National Industrial Research Institute of Nagoya (Japan) with support of the PWING project (JSPS KAKENHI 16H06286).

REFERENCES

1. Guglielmi, A.V., Troitskaya, V.A. (1973) Geomagnetic pulsations and diagnostics of the magnetosphere. M.: Nauka.
2. Guglielmi, A.V. (1979) MHD waves in near–Earth plasma. M.: Nauka.
3. Kangas, J., Guglielmi, A., Pokhotelov, O. (1998) Morphology and Physics of Short-Period Magnetic Pulsations. (Review). Space Science Reviews, 83: 435-512. http://dx.doi.org/10.1023/A:1005063911643.
4. Fukunishi, H., Toya, T., Koike, K., Kuwashima, M., Kawamura, M. (1981) Classification of hydromagnetic emissions based on frequency-time spectra. J. Geophys. Res., v. 86, No. A11: 9029-9039, https://doi.org/10.1029/JA086iA11p09029.
5. An, Z., Zonca, F., Tao, .X, Chen, L. (2023) Frequency chirping of electromagnetic ion cyclotron waves in Earth's magnetosphere. arXiv:2303.07799v1 [physics.space-ph].
6. Anisimov, S.V., Dmitriev, E.M., Afinogenov, K.V., Guryev, V.A. (2011) Geomagnetic observations at Borok Geophysical Observatory. Bulletin of ONZ (Earth Sciences Division+) RAS, 3, NZ5002, https://doi.org/10.2205/2011NZ000104.
7. SpectraPLUS-DT - Pioneer Hill Software 2022 https://www.cetaceanresearch.com/documents/SpectraPLUS-DT-Options.pdf.
8. Levshin, A.L., Frantsuzova, V.M., Shkadinskaya, G.V. (1968) Spectral-temporal analysis of seismic waves. Computational seismology. M., issue 4: p. 197.
9. Torr, M.R., Torr, D.G., Zukic, M., et al. (1995) A far ultraviolet imager for the International Solar-Terrestrial Physics Mission. Space Sci Rev 71: pp. 329–383. https://doi.org/10.1007/BF00751335.
10. Gjerloev, J.W. (2012) The SuperMAG data processing technique. J. Geophys. Res. 117 A09213.https://doi.org/10.1029/2012JA017683.
11. Eselevich, V.G., Parkhomov, V.A. (2023) Role of alpha particles in penetration of solar wind diamagnetic structures into the magnetosphere. Solar-Terrestrial Physics, v. 9 issue 3: 1–20. https://doi.org/10.12737/stp-93202302.
12. Akasofu, S.I. (2017) Auroral Substorms: Search for Processes

Vol. 63 No 04(248) 2023
DOI: https://doi.org/10.5564/pmas.v63i04.3430

Causing the Expansion Phase in Terms of the Electric Current Approach. Space Sci Rev. 212: pp. 341–381. https://doi.org/10.1007/s11214-017-0363-7.

13. Kodera, K., Gendrin, R., de Villedary, C. (1977) Complex representation of a polarized signal and its application to the analysis of ULF waves, J. Geophys. Res. 82 (7): pp. 1245-1255.https://doi.org/10.1029/JA082i007p01245.

14. Li, W., Thorne, R.M., Bortnik, J., Shprits, Y.Y., Nishimura, Y., Angelopoulos, V., Chaston, C., Le Contel, O., Bonnell, J.W. (2011) Typical properties of rising and falling tone chorus waves. Geophys. Res. Lett. 38, L14103, https://doi.org/10.1029/2011GL047925.

15. Tsurutani, B.T., Smith, E.J. (1974) Postmidnight chorus: A substorm phenomenon, J. Geophys. Res. 79 (1): pp. 118– 127. https://doi.org/10.1029/JA079i001p00118.

16. Shen, X.C., Li, W., Ma, Q. (2021) Periodic rising and falling tone ECH waves from Van Allen Probes observations. Geophysical Research Letters 48: e2020GL091330. https://doi.org/10.1029/2020GL091330.

17. Anistratenko, A.A., Ponomarev, E.A. (1981) Simulating conditions of corpuscular precipitation and electric currents zones in the nightside polar magnetosphere. Research of geomagnetism, aeronomy and solar physics. M. Nauka, 53: pp. 15–26.

18. Ponomarev, E.A. (1983) Mechanisms of magnetospheric substorms. M., Nauka, p. 157.

19. Mishin, V.V., Lunyushkin, S.B., Mikhalev, A.V., Klibanova, Yu.Yu., Tsegmed, B. (2018) Extreme Geomagnetic and Optical Disturbances over Irkutsk during the 2003 November 20 Superstorm. Journal of Atmospheric and Solar-Terrestrial Physics 151 pt. A: pp. 68–78. https://doi.org/10.1016/j.jastp.2018.10.013

20. Angelopoulos, V. (2008) The THEMIS mission. Space Sci. Rev. 141: pp. 5-34. https://doi.org/10.1007/s11214-008-9336-1.

21. Tsegmed, B., Potapov, A., Baatar, N. (2022) Daytime geomagnetic pulsations accompanying sudden impulse of solar wind. Proceedings of the Mongolian Academy of Sciences 62 02: p. 242. https://doi.org/10.5564/pmas.v62i02.2380.

22. Horita, R.E., Barfield, J.N., Heacock, R.R., Kangas, J. (1979), IPDP Source Region and resonance proton energies. J. Atmos. Terr. Phys. 41: p. 293. https://doi.org/10.1016/0021-9169(79)90112-0/

23. Sucsdorff, E. (1936). Occurance of rapid Micropulsations at Sodankuld during 1932 to 1935. Terrestr. Magn. Atmospheric Electr. 41, p. 337. https://doi.org/10.1029/TE041i004p00337.